tween annual net ice accumulation and net ablation at the surface and is located at the upper elevation of bare ice (without refrozen firn or superimposed ice) at the end of the summer melt season. The empirical equation for the equilibrium-line altitude (ELA) is a decreasing quadratic function of latitude (*43*) that gives an ELA of 1418 m at the latitude of the Swiss Camp. The camp was established in 1990 at the nominal location of the equilibrium line, based on surface observations in previous years (*29*). It lies on a small ridge, and local variations in the altitude of the equilibrium zone range from around 1200 m at the camp to 1400 m south of the camp.
17. Measured by University of Kansas ice-penetrating radar. Data are available online at http://tornado.rsl.ku.edu/1998thick.htm.
18. W. L. Wang, H. J. Zwally, W. Abdalati, S. Luo, *Ann. Glaciol*., in press, using the measured ice thickness of 1220 m. The modeled basal temperature is slightly below the PMP at the ice divide and is essentially at the PMP along a flowline from 400 km above the camp to the ice edge.
19. M. Luthi, M. Funk, A. Iken, S. Gogineni, M. Truffer, *J. Glaciol*., in press, obtained a ratio of basal sliding of 60% in the lateral shear zone of Jakobshavn Isbrae, but noted that such a high ratio is probably not representative for the ice sheet.
20. GPS data were recorded by a geodetic-quality dual-frequency Trimble 4000 SSi receiver (Trimble, Sunnyvale, CA), which is inside an insulated box in a camp tent and powered by four to six 100–a-h batteries and two 18-W solar panels. The 2-m extension of the antenna above the ice keeps the antenna above the seasonal snow accumulation, which ranges from about 0.5 to 1.8 m interannually. Yearly data were downloaded when the camp was occupied each May. Data collection ended in the fall of 1999 because of anomalous behavior of the receiver.
21. During the spring occupation of the Swiss Camp, data were usually recorded continuously instead of once every 10 to 15 days. To avoid large velocity errors for short time intervals, the following position data for multiple 12-hour time periods were averaged: 23 to 29 May 1998 (13 periods), 23 to 28 May 1999 (10 periods), and 9 and 10 June 1999 (4 periods).
22. R. W. King, *Documentation of the GAMIT GPS Analysis Software Version 10.05* (2001); and T. A. Herring, *Documentation of the GLOBK Software Version 5.1* (2001), MIT, Cambridge, MA. See also http://www-gpsg.mit.edu/~simon/gtgk. The Cartesian coordinates of the antenna were calculated, relative to bedrock sites at Thule Air Force Base, Kellyville, and Kulusuk in Greenland, from 12-hour increments of data. The average standard deviations of the coordinates calculated with GLOBK is 1.2 cm horizontally and 3.3 cm vertically. The standard deviations of the north and east components of the positions are somewhat higher during the winter periods (e.g., the standard deviation of the north component went from a base value of about 0.5 cm to a high of nearly 6 cm during the winter of 1999). The large uncertainties occurred on days when only the bedrock site at Thule was operating and when less than 12 hours of data were recorded at Swiss Camp. Times assigned to the points are the midpoints of the times of the data increments. The overall average standard deviation of the horizontal velocity is 0.14 cm/day. Analysis techniques are also described in (*44*).
23. The horizontal velocity at markers 2.15 km downstream from Swiss Camp is 0.67 cm/day slower than at the camp. Therefore, as the camp moved from 1996 to 1999, the estimated decrease in horizontal velocity was 0.036 cm/day/year, or 0.14 cm/day during the 4-year period.
24. The respective advancements and reductions for 1997, 1998, and 1999 were: 1.8 and 0.8 m, 2.5 and 1.6 m, and 2.9 and 1.9 m.
25. W. Abdalati, K. Steffen, *J. Geophys. Res.* **106**, 33983 (2001).
26. PDD = $\sum_i \alpha_i T_i/24$, where T_i are hourly averaged near-suface air temperatures, $\alpha_i = 1$ if $T_i > 0$, and $\alpha_i = 0$ if $T_i \leq 0$.
27. The year-to-year ratios of cumulative PDDs to melt areas (*19*) differ from unity by less than 19%. The Jacobshavn melt region is defined from about 65.5 to 76°N and from the western ice edge to the divide. The respective cumulative melt-days obtained from passive microwave for the area near the camp are 30, 60, 97, and 47. The year-to-year correspondence for the camp location is not as good (ratios differ from unity by up to 33%), probably because the passive-microwave index of melt days records only the occurrence of surface melting, whereas the deg-days index registers more for warm days (e.g., 5 times more for +5°C) than for days that are just above the melting point. In contrast, the melt-area index used for the Jacobshavn region is also sensitive to the intensity of melting, which expands the area of melting to higher elevations.
28. R. J. Braithwaite, O. B. Olesen, in *Glacier Fluctuations and Climate Change*, J. Oerlemans, Ed. (Kluwer, Dordrecht, Netherlands, 1989), pp. 219–233.
29. H. H. Thomsen, L. Thorning, R. J. Braithwaite, *Glacier-Hydrological Conditions on the Inland Ice North-East of Jakobshavn/Ilusissat, West Greenland: Report 138* (Gronlands Geologiske Undersogelse, Copenhagen, Denmark, 1998).
30. For example, data for 1997 through 1999 from the Automated Weather Station (AWS) (*15*) at JAR-1 at a 960-m elevation and 16.3 km downstream from the camp show that the lag in melting onset between the sites varies from only 1 to 14 days until about 30 deg-days are cumulated. The end of melting may occur even closer in time at different elevations in the ablation zone. In 1999 at least, the cessation was almost simultaneous at Swiss Camp, JAR-1, and JAR-2, which is at a 528-m elevation and 17.1 km downstream from JAR-1.
31. G. de Q. Robin, *J. Glaciol.* **13**, 543 (1974).
32. At the JAR-1 AWS site, which was located near the side of a lake hundreds of meters in diameter, the sonic surface-height data show that the surface level dropped 1.5 m in a few hours on 17 July 1996 as the water drained from the ice. A similar drop of 0.8 m occurred on 25 June 1997, when the station had moved 70 m closer to the lake edge.
33. A. Iken, H. Rothlisberger, A. Flotron, W. Haberli, *J. Glaciol.* **29**, 28 (1983).
34. C. F. Raymond, *J. Geophys. Res.* **92**, 9121 (1987).
35. J. T. Houghton *et al.*, Eds., *Climate Change 2001: The Scientific Basis* (IPCC Report, Cambridge, UK, 2001).
36. R. J. Braithwaite, O. B. Olesen, *Ann. Glaciol.* **14,** 20 (1990).
37. P. U. Clark, R. B. Alley, D. Pollard, *Science* **286**, 1103 (1999).
38. R. M. Koerner, *Science* **244**, 964 (1989).
39. N. Reeh, *Nature* **317**, 797 (1985).
40. _____, O. B. Olesen, *Ann. Glaciol.* **8**, 146 (1986).
41. I. Joughin, S. Tulaczyk, M. Fahnestock, R. Kwok, *Science* **274**, 228 (1996).
42. J. J. Mohr, N. Reeh, S. Madsen, *Nature* **391**, 273 (1998).
43. H. J. Zwally, M. B. Giovinetto, *J. Geophys. Res.* **106**, 33717 (2001).
44. K. Larson, J. Plumb, J. Zwally, W. Abdalati, *Polar. Geogr.* **25**, 22 (2002).
45. Supported by NASA's ICESat (Ice Cloud and Land Elevation Satellite) science activities and Cryospheric Sciences Program.

9 April 2002; accepted 30 May 2002
Published online 6 June 2002;
10.1126/science.1072708
Include this information when citing this paper.

Super ENSO and Global Climate Oscillations at Millennial Time Scales

Lowell Stott,[1]* Christopher Poulsen,[1] Steve Lund,[1] Robert Thunell[2]

The late Pleistocene history of seawater temperature and salinity variability in the western tropical Pacific warm pool is reconstructed from oxygen isotope ($\delta^{18}O$) and magnesium/calcium composition of planktonic foraminifera. Differentiating the calcite $\delta^{18}O$ record into components of temperature and local water $\delta^{18}O$ reveals a dominant salinity signal that varied in accord with Dansgaard/Oeschger cycles over Greenland. Salinities were higher at times of high-latitude cooling and were lower during interstadials. The pattern and magnitude of the salinity variations imply shifts in the tropical Pacific ocean/atmosphere system analogous to modern El Niño–Southern Oscillation (ENSO). El Niño conditions correlate with stadials at high latitudes, whereas La Niña conditions correlate with interstadials. Millennial-scale shifts in atmospheric convection away from the western tropical Pacific may explain many paleo-observations, including lower atmospheric CO_2, N_2O, and CH_4 during stadials and patterns of extratropical ocean variability that have tropical source functions that are negatively correlated with El Niño.

The discovery that the Earth experiences large, abrupt climate variations that have no clear external (solar) forcing has stimulated the pursuit of highly resolvable climate archives such as ice, marine, and terrestrial deposits that can provide clues about the origin of these rapid climate events. Until recently, too few records existed from the tropics to establish whether millennial climate variability is inherently tied to tropical climate dynamics. This void is being filled with new sediment cores collected by the IMAGES program (*1*).

[1]Department of Earth Sciences, University of Southern California, 3651 Trousdale Parkway, Los Angeles, CA 90089, USA. [2]Department of Geological Science, University of South Carolina, 700 Sumter Street, Columbia, SC 29208, USA.

*To whom correspondence should be addressed. E-mail: stott@usc.edu

Western Tropical Pacific Proxy Records

Here, we present $\delta^{18}O$ and Mg/Ca paleothermometry results [see supporting online material (SOM)] from surface-dwelling planktonic foraminifera from a site with a high sediment accumulation rate (MD98-2181, hereafter MD81) located at the eastern edge of the Indonesian archipelago at 6.3°N and 125.83°E (at a 2114-m water depth) (Fig. 1). The data are used to investigate whether sea surface temperatures (SSTs) in the Pacific warm pool varied in association with high-latitude climate during the past 70 thousand years (kyrs). If they did, this would have important implications for understanding millennial climate variability, because the Pacific warm pool is an important center of atmospheric convection. During the northern summer, modern SSTs in the warm pool average 29° to 30°C. In winter, SSTs cool to 27° to 26°C. Precipitation is highest in summer, with roughly 80% of annual rainfall occurring between June and October (*2*). Rainfall averages between 300 and 400 mm/month during summer and between 50 and 100 mm/month during winter. As a result of this precipitation pattern, sea surface salinities vary seasonally by about 1.5 per mil (‰). The annual precipitation pattern is tied to the migration of the Intertropical Convergence Zone (ITCZ) over the site and the timing of the northern monsoon. During modern El Niños and La Niñas, the western tropical Pacific experiences dramatic differences in precipitation. For example, summer precipitation over northern Indonesia can be diminished by as much as 60% during a major El Niño.

ENSO-induced changes in surface temperature and precipitation leave a measurable signal in the trace element and $\delta^{18}O$ composition of biogenic carbonate precipitated in surface waters. Shallow water corals are excellent recorders of this geochemical variability and provide unparalleled resolution for reconstructing ENSO (*3*–*5*). However, there are no coral records from the Indonesian region that extend throughout the entire last glacial cycle, and most glacial age corals are now well below sea level and beyond the reach of conventional coring, except where they have been uplifted by tectonism (*6*). Planktonic foraminifera are also excellent archives of surface water hydrography and can be recovered from long sediment cores that extend continuously through the last glacial. *Globigerinoides ruber* and *Globigerinoides sacculifer*, two surface-dwelling species of foraminifera that have been used extensively in paleoceanographic reconstructions, occur in marine sediments of the western tropical Pacific. In plankton tow studies (*7*), *G. ruber* is abundant in the warm summer surface waters of the western tropical Pacific that can reach 30°C. Conversely, *G. sacculifer* does not produce shells readily at temperatures higher than about 27°C (*8*). On the other hand, this species does occur in the sediment records from Indonesia as a distinct but low abundant constituent, implying that it produces shells primarily during cooler winter months when temperatures average 26° to 27°C. Analyses of recent and late Holocene *G. ruber* and *G. sacculifer* extracted from site MD81 display $\delta^{18}O$ and Mg/Ca paleotemperatures that reflect these seasonal preferences [see SOM (fig. S1)]. Calcite preservation is excellent in these cores. The core sits above the lysocline, as attested to by the occurrence of aragonite pteropods throughout the core. The consistency between the isotopic- and Mg/Ca-based foraminiferal SST reconstructions suggests that each proxy provides a good estimate of seasonal surface water conditions.

The age model for the early Holocene and late glacial intervals of MD81 is based on 10 accelerator mass spectrometry dates [see SOM (fig. S2 and table S1)]. The age model for the glacial portion of this core is based on correlation of the $\delta^{18}O$ of *G. ruber* and the Greenland Ice Sheet Project Two (GISP2) ice core $\delta^{18}O$ stratigraphy (*9*). We use discrete horizons in the $\delta^{18}O$ stratigraphy in MD81 to correlate directly with GISP2 (see SOM).

Using a minimum number of tie points and extrapolating a nearly constant rate of sediment accumulation between them produces a $\delta^{18}O_{VPDB}$ stratigraphy for MD81 that is remarkably similar in character to the $\delta^{18}O_{SMOW}$ stratigraphy in GISP2 (Fig. 2). Within the glacial portion of MD81, each of the major Dansgaard/Oeschger (D/O) events can be identified in the $\delta^{18}O$ record (Fig. 2). Both planktonic foraminiferal species record the isotopic variability associated with the D/O cycles, although the $\delta^{18}O$ of *G. sacculifer* is offset from that of *G. ruber*, and the sample resolution is not yet as high. The close correspondence between Greenland and MD81 $\delta^{18}O$ records implies that, on time scales of D/O cycles, the tropics were undergoing changes in both summer and winter conditions, with warmer seasonal temperatures and/or lower local salinities occurring during interstadials.

Reconstructing Tropical SSTs

The Mg/Ca paleotemperatures for *G. ruber* and *G. sacculifer* (Fig. 3) display systematic shifts between the Holocene and last glacial that are similar to other tropical Pacific records (*10*). Summer *G. ruber* temperatures were between 26° and 27°C during the last glacial maximum (LGM), or approximately 2°C cooler than Holocene temperatures (Fig. 3). Winter *G. sacculifer* temperatures were approximately 3°C cooler during the glacial; however, the warmest *G. sacculifer* temperatures occurred in the early Holocene. The magnitude of summer and winter SST variability was quite small throughout the past 70 kyrs, averaging only 1° to 2°C throughout most of the last glacial period.

The Local Salinity Record

The small amplitude of temperature variability in the glacial portion of MD81 does not account for the larger changes in planktonic foraminifer $\delta^{18}O$ or the strong correspondence between the MD81 and Greenland $\delta^{18}O$ records. The planktonic record does contain a component of $\delta^{18}O$ variability that reflects changes in ice volume. However, this has a longer time constant than the millennial-length variations, and the magnitude of this effect can be constrained from the $\delta^{18}O$ of atmospheric O_2 from ice cores (*11*, *12*). The close correspondence between MD81 $\delta^{18}O$ variations and the GISP2 record must reflect local hydrographic changes that affected local surface water $\delta^{18}O$ and salinity.

To estimate how surface-water $\delta^{18}O$ and salinity varied during the last glacial, we differenced the Mg/Ca-derived and $\delta^{18}O$-derived SST estimates (holding the $\delta^{18}O$ of surface water

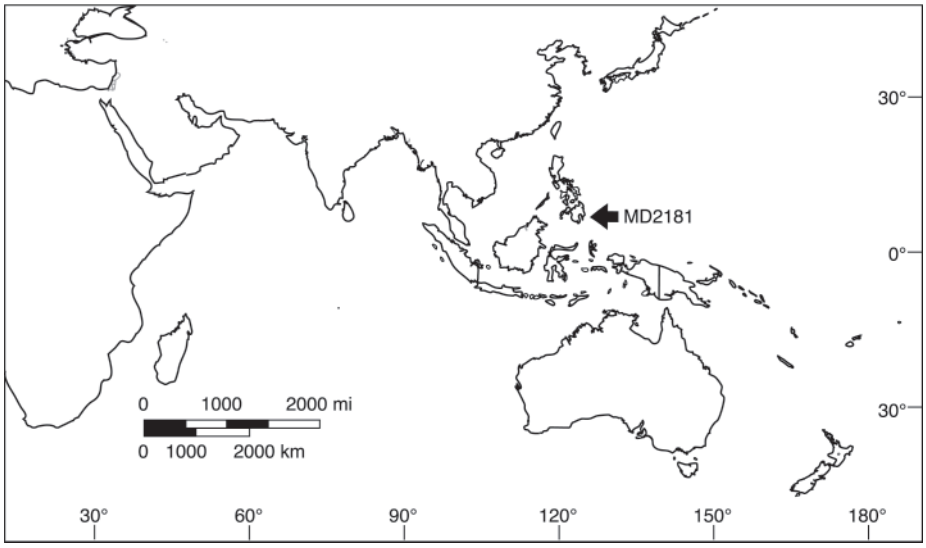

Fig. 1. Map showing location of MD98-2181.

constant at the modern value of [−0.4‰ Pee Dee belemnite (PDB) standard]. The difference in these two estimates is transformed to an isotopic difference between modern and glacial seawater $\delta^{18}O$ ($\Delta\delta^{18}O$) by dividing the difference between the $\delta^{18}O$-derived and the Mg/Ca-derived paleotemperature (Δ temperature) by the temperature-dependent fractionation of 0.22‰/°C. We refer to this as $\Delta\delta^{18}O$ to reflect the change in surface water isotopic composition relative to the modern value. Where $\Delta\delta^{18}O$ exceeds the ice volume component, we interpret this to reflect higher (higher surface water $\delta^{18}O$) or lower (lower surface water $\delta^{18}O$) surface salinities at this site (Fig. 4).

It is evident from the comparison of $\Delta\delta^{18}O$ and the GISP2 temperature record that much of the Indonesian planktonic foraminiferal calcite $\delta^{18}O$ signal was associated with changes in local salinity. The modern $\delta^{18}O$-salinity relationship in the tropical western Pacific is approximately 0.2‰ ($\delta^{18}O$)/‰ salinity (*13*), although this relationship varies slightly from region to region and may be lower in the western tropical Pacific. After accounting for the ice volume effect and applying the modern $\delta^{18}O$-salinity relationship, the $\Delta\delta^{18}O$ results imply that summer surface salinities during the glacial were as much as 2‰ higher than they are today. A similar estimate of glacial-Holocene salinity contrast has been observed in other warm pool records (*14*). Thus, higher sea surface salinities appear to have been widespread within the warm pool. Because surface water salinities are strongly correlated with precipitation patterns in the warm pool and because precipitation in northern Indonesia is heavily weighted toward the summer months, we interpret these results to reflect a shift in mean precipitation that affected the local hydrologic balance during summer, producing the higher surface water $\delta^{18}O$. Consequently, the summer/winter salinity contrast was smaller.

The most remarkable feature of the MD81 record is the correlation between $\Delta\delta^{18}O$ and the D/O cycles in Marine Isotope Stage III (MIS III) (Fig. 4). Positive excursions in $\Delta\delta^{18}O$, reflecting increased tropical salinities, coincided with stadial conditions at high latitudes. The interstadials were associated with lower tropical salinities. The magnitude of $\Delta\delta^{18}O$ variability during the D/O cycles was on the order of 0.5 to 1.0‰, equivalent to 1 to 2‰ salinity (approximately the magnitude of the modern seasonal variability). Comparing the $\Delta\delta^{18}O$ variations in the MD81 to the global ocean $\Delta\delta^{18}O$ record derived from the ice core O_2 record (*12*) indicates that the positive excursions in MD81 $\Delta\delta^{18}O$ reflect increased surface salinities relative to modern values. This implies that, in the western tropical Pacific, salinities were, on average, saltier throughout much of the past 70 kyrs than they are today. Only during interstadials did summer salinities increase modestly, but they never returned completely to modern values.

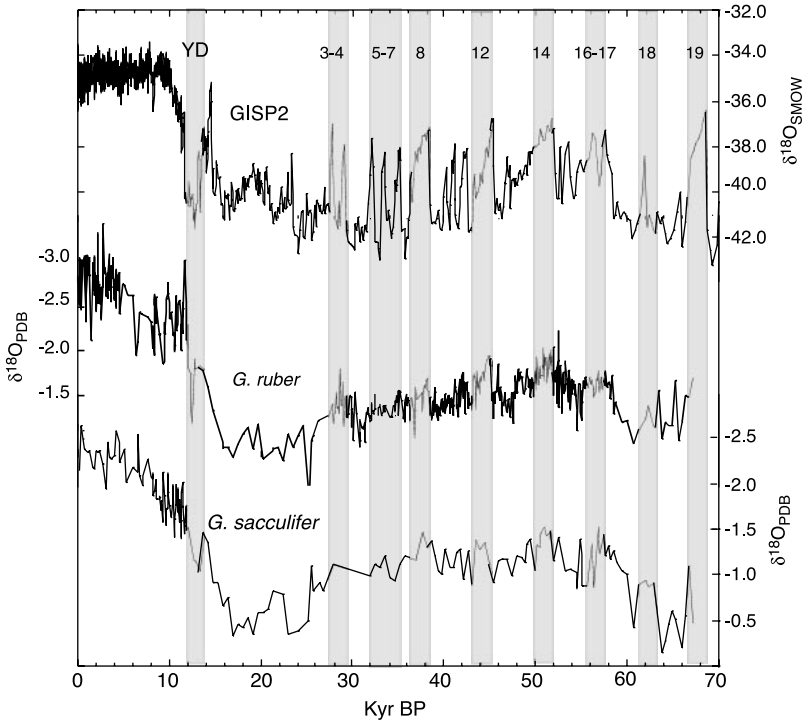

Fig. 2. The $\delta^{18}O$ of Greenland Ice (GISP2), as compared to the $\delta^{18}O$ of planktonic foraminifera from MD81. Interstadial numbers and the Younger Dryas are indicated at the top.

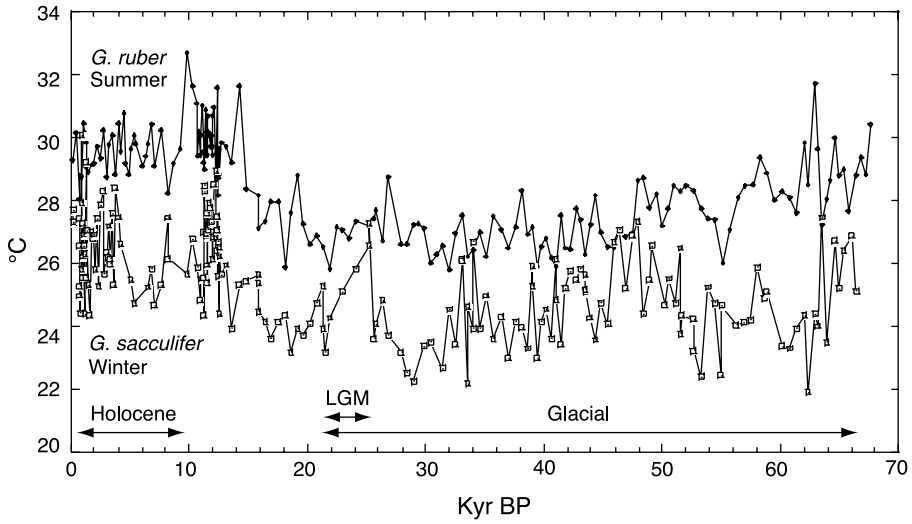

Fig. 3. Mg/Ca paleo-SST reconstructions for summer and winter.

A Pleistocene Pattern of El Niño and La Niña on Millennial Time Scales

The magnitude of SST and salinity variability in the western tropical Pacific implicates a pattern of shifting atmospheric convection away from the western tropical Pacific when the high latitudes were colder. This is analogous to modern ENSO, where the region of strongest vertical convection shifts away from Indonesia toward the central equatorial Pacific during an El Niño. However, today strong El Niños typically last less than a year (*15*, *16*). The MD81 record points to longer term shifts in the mean state of atmospheric convection over the western tropical Pacific that lasted for millennia. Because of the way foraminifer samples average a signal, the millennial changes could also reflect more frequent and perhaps more severe El Niños, whereas the interstadials were associated with less frequent and less severe ENSO events. In this way, the signal left in the sediments is weighted toward the mean or more frequent condition. We apply the term "super-ENSO" to distinguish our inference about the millennial patterns seen in the tropics from our knowledge of modern ENSO, which is explicitly tied to interannual variability.

The correlation between stadial conditions at high latitudes and El Niño in the tropics is surprising, because previous proposals have suggested a possible El Niño–stadial relation (*17*–*19*). This stems from observations that El Niño can have a far-reaching effect, including generally warmer conditions in the extratropics (*20*). We submit that a review of existing data for the last glacial indicates that tropical and extratropical climate/ocean variability is consistent with a dominant El Niño state in the western tropical Pacific during stadials and that the brief interstadials coincided with near-normal or La Niña conditions. Below, we review records that exhibit D/O associations and point out how these records provide a consistent link between El Niño and stadials.

Tropical Records

In the Indian Ocean, upwelling along the Oman margin results from southerly monsoon winds during the summer. Productivity is highest in summer in response to wind-driven upwelling, leading to denitrification in the water column (*21*). Recently, Altabet *et al*. (*21*) showed that wind-driven upwelling and productivity along the Oman margin varied in concert with the D/O cycles. Denitrification was reduced during stadials and increased during interstadial times. A $\delta^{18}O$ stalagmite record from Hulu cave in eastern China has also revealed a pattern of reduced summer monsoon moisture at times when Greenland was experiencing stadial conditions, consistent with the Oman margin record of millennial-scale monsoon failure (*22*). Today, monsoon failure and El Niño are strongly correlated, and we submit that this provides a coherent explanation for the coincident changes in the Indian and Asian summer monsoons during stadial periods.

The Pleistocene record of denitrification in the eastern tropical North Pacific (*23*–*25*) is very similar to that of the Indian Ocean (*21*). Denitrification was reduced during stadial periods, implying a less intense oxygen minimum zone (OMZ). Because the OMZ in this region is maintained by high productivity due to trade wind–induced upwelling, the diminution of OMZ during stadial periods suggests that the trade winds were weaker at those times. Modern El Niños are associated with weakened trade winds and reduced productivity in the eastern tropical Pacific.

The glacial record from Cariaco Basin in the western equatorial Atlantic exhibits variations between laminated and bioturbated sedimentation that correlate with the millennial climate oscillations in Greenland (*26*). Intervals of bioturbated sedimentation coincided with stadials, and laminated intervals coincided with interstadials. The bioturbated sediments reflect periods of lower productivity and reduced rainfall and runoff (*26*). Disruptions in convection over the western tropical Pacific during modern ENSO results in reduced rainfall and runoff in Cariaco as the seasonal migration of the ITCZ is interrupted. The brief return of laminated sediments during interstadials reflects periods of normal or higher rainfall, runoff, and higher productivity, a pattern associated with the normal or La Nina phase of ENSO.

In the tropical Pacific, Lea *et al*. (*10*) used Mg/Ca and $\delta^{18}O$ to reconstruct changes in surface water $\delta^{18}O$ during the last 130,000 years. Although the record they studied from Ontong Java Plateau is of low resolution, they documented a smaller glacial-Holocene $\Delta\delta^{18}O$ (0.7‰) than we observe in Indonesia and smaller than they observed in their eastern tropical Pacific site. They suggested that the smaller change in the western Pacific could be explained by stronger trade winds and enhanced vapor transport to the western Pacific. These results would appear to be in conflict with those presented here. However, the Ontong Java Plateau site lies at the edge of the central equatorial salinity anomaly associated with modern ENSO (*4*, *27*). During an El Niño, the locus of atmospheric convection shifts eastward across the Ontong Java Plateau (*27*). This site may have been within the zone of enhanced precipitation as convection shifted eastward away from Indonesia during the stadials.

Extratropical Records

In the northeastern Pacific, the Santa Barbara Basin contains a record of marine variability that matches the Greenland temperature record (*28*). In this basin, periods of laminated sedimentation correlate with interstadials, whereas bioturbated intervals correlate with stadials. We again call upon a tropical link to explain this sedimentation pattern. Today, low sea level pressure and strong atmospheric convection in the western tropical Pacific are accompanied by higher sea level pressure in the northeastern Pacific (*29*). During an El Niño, reduced convection over the western tropical Pacific leads to a weakened NE Pacific high. As a result, northerly wind stress along the California margin is reduced, leading to diminished productivity, less carbon oxidation, and higher dissolved oxygen in the marginal basins. Shifts such as this have been implicated in recent reversals in the laminated sedimentation patterns of the Santa Barbara and Santa Monica Basins (*30*). An El Niño–stadial relation provides a logical explanation for reduced productivity and carbon oxidation that resulted in higher oxygen levels within the Santa Barbara Basin during the cold periods.

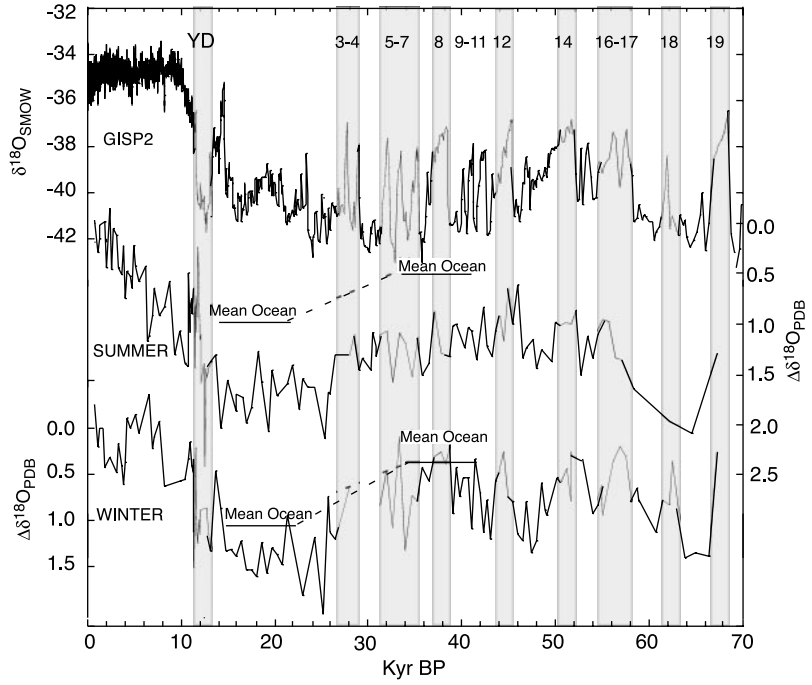

Fig. 4. The $\Delta\delta^{18}O$ of planktonic foraminifera, as compared to the GISP2 $\delta^{18}O$ record (D/O events are labeled at the top). The component of $\Delta\delta^{18}O$ due to ice volume differences at MIS III and MIS II is shown. The $\Delta\delta^{18}O$ variations that exceed the ice volume value reflect local surface water $\delta^{18}O$ differences relative to today. Increased $\Delta\delta^{18}O$ reflects increased salinity. Summer salinities were as much as ~2‰ higher during the LGM, whereas winter salinities were similar to modern values. The largest salinity variations in both summer and winter were associated with the D/O cyclicity. Stadials were associated with higher salinities during both summer and winter. During the interstadials, surface salinities were similar to modern or, in the case of winter values, were slightly lower than today.

Atmospheric CO_2 and N_2O

The most compelling argument for an El Niño–stadial link may be the atmospheric CO_2, CH_4, and N_2O records from ice cores (*31*–*33*). The atmospheric concentration of each of these gas species increased during interstadials, although the variations were small. The primary source of preindustrial atmospheric N_2O, CH_4, and CO_2 is from the tropics. Upwelling in the tropical Pacific is the largest atmospheric source of CO_2 and a major source of N_2O (*32*). Tropical soils constitute the other primary source of N_2O, and these are major sources of CH_4. El Niño events disrupt the flux of CO_2 and N_2O to the atmosphere as upwelling in the eastern equatorial Pacific is reduced or shut down. Similarly, shifts in precipitation from land to ocean, as occurs during El Niño, can have a profound effect on tropical soils, as witnessed by the severe droughts over Indonesia and failure of the monsoon. We submit that the El Niño–stadial association provides a plausible explanation for the lower atmospheric CO_2, CH_4, and N_2O observed in ice core records.

We conclude that the strongest case can be made for an El Niño–stadial linkage during the last 70 kyrs. At times of cooling at high latitudes, the tropical Pacific was experiencing either less-frequent or less-persistent El Niños. The notion that El Niño would have been the dominant state during a glacial contrasts sharply with previous modeling and low-resolution observational studies that have predicted stronger trade winds and a larger tropical thermocline tilt under glacial conditions (*34*, *35*). The new perspective on millennial climate variability in the tropics presents an important challenge to the climate community to find the physical forcing that causes reduced atmospheric convection in the western tropical Pacific and reduced trade wind strength at times of high-latitude cooling. The answers will likely shed important light on how and why the Earth's climate undergoes abrupt climate changes and the likelihood that an abrupt change will occur in the future.

References and Notes

1. B. K. Lindsley, *Nature* **380**, 243 (1996).
2. Data from the NOAA-CIRES Climate Diagnostics Center, Boulder, CO, available online at www.cdc.noaa.gov/.
3. M. K. Gagan *et al*., *Quat. Sci. Rev*. **19**, 45 (2000).
4. F. E. Urban, J. E. Cole, J. T. Overpeck, *Nature* **407**, 989 (2000).
5. D. P. Schrag, *Paleoceanography* **14**, 97 (1999).
6. A. W. Tudhope *et al*., *Science* **291**, 1511 (2001).
7. S. R. Troelstra, D. Kroon, *Neth. J. Sea Res*. **24**, 459 (1989).
8. D. Caron, personal communication based on live collections in Bermuda.
9. T. Sowers *et al*., *Paleoceanography* **8**, 737 (1993).
10. D. W. Lea, D. K. Pak, H. J. Spero, *Science* **289**, 1719 (2000).
11. M. Bender, T. Sowers, L. Labeyrie, *Global Biogeochem. Cycles* **8**, 363 (1994).
12. N. J. Shackleton, *Science* **289**, 1897 (2000).
13. R. G. Fairbanks *et al*., *Coral Reefs* **16**, 593 (1997).
14. J. I. Martinez, P. D. Deckker, A. R. Chivas, *Mar. Micropaleontol*. **32**, 311 (1997).
15. S. G. H. Philander, *El Niño, La Niña, and the Southern Oscillation* (Academic Press, New York, 1990).
16. M. J. McPhaden, *Science* **283**, 950 (1999).
17. M. A. Cane, *Science* **282**, 5386 (2002).
18. M. A. Cane, A. C. Clement, in *Mechanisms of Global Climate Change at Millennial Time Scales*, P. U. Clark, R. S. Webb, L. D. Keigwin, Eds., vol. 112 of Geophysical Monograph Series (American Geophysical Union, Washington, DC, 1999), pp. 373–384.
19. A. C. Clement, M. A. Cane, in *Mechanisms of Global Climate Change at Millennial Time Scales*, P. U. Clark, R. S. Webb, L. D. Keigwin, Eds., vol. 112 of Geophysical Monograph Series (American Geophysical Union, Washington, DC, 1999).
20. M. Cane, *Science* **282**, 59 (1998).
21. M. A. Altabet, M. J. Higginson, D. W. Murray, *Nature* **415** (2002).
22. Y. J. Wang *et al*., *Science* **294**, 2345 (2001).
23. E. Emmer, R. C. Thunell, *Paleoceanography* **15**, 377 (1999).
24. R. S. Ganeshram, T. F. Pederson, S. E. Calvert, R. Francois, *Nature* **215**, 156 (2002).
25. C. Pride *et al*., *Paleoceanography* **14**, 397 (1999).
26. L. C. Peterson, G. H. Haug, K.A. Hughen, U. Röhl, *Science* **290**, 1950 (2000).
27. National Center for Environmental Prediction, NOAA Web site www.cpc.ncep.noaa.gov.
28. R. J. Behl, J. P. Kennett, *Nature* 379, 243 (1996).
29. F. B. Schwing, P. M. Green, T. Murphree, *EOS* **80**, 262 (1999).
30. L. D. Stott *et al*., *Nature* **407**, 367 (2000).
31. T. Blunier *et al*., *Nature* **394**, 739 (1998).
32. J. Flückiger *et al*., *Science* **285**, 227 (1999).
33. B. Stauffer *et al*. *Nature* **392**, 59 (1998).
34. A. B. G. Bush, S. G. H. Philander, *Science* **279**, 1341 (1998).
35. D. Andreasen, D. H., A. C. Ravelo, A. J. Broccoli, *J. Geophys. Res*. **106,** 879 (2001).

36. We thank the NSF for supporting this research. We acknowledge the careful analytical assistance of M. Rincon.

Supporting Online Material

www.sciencemag.org/cgi/content/full/297/5579/222/DC1
Materials and Methods
Figs. S1 to S3
Table S1
References and Notes

7 March 2002; accepted 22 May 2002

REPORTS

El Niño–Like Pattern in Ice Age Tropical Pacific Sea Surface Temperature

Athanasios Koutavas,[1]* Jean Lynch-Stieglitz,[1] Thomas M. Marchitto Jr.,[1] Julian P. Sachs[2]

Sea surface temperatures (SSTs) in the cold tongue of the eastern equatorial Pacific exert powerful controls on global atmospheric circulation patterns. We examined climate variability in this region from the Last Glacial Maximum (LGM) to the present, using a SST record reconstructed from magnesium/calcium ratios in foraminifera from sea-floor sediments near the Galápagos Islands. Cold-tongue SST varied coherently with precession-induced changes in seasonality during the past 30,000 years. Observed LGM cooling of just 1.2°C implies a relaxation of tropical temperature gradients, weakened Hadley and Walker circulation, southward shift of the Intertropical Convergence Zone, and a persistent El Niño–like pattern in the tropical Pacific. This is contrasted with mid-Holocene cooling suggestive of a La Niña–like pattern with enhanced SST gradients and strengthened trade winds. Our results support a potent role for altered tropical Pacific SST gradients in global climate variations.

Studies of El Niño–Southern Oscillation (ENSO) dynamics and impacts demonstrate that the tropical Pacific ocean-atmosphere system influences global climate on interannual to decadal time scales (*1*). Models suggest that this system is sensitive to orbital forcing, dominated by precession in the tropics, which modulates the annual insolation cycle and affects the seasonal strength of winds and intensity of upwelling (*2*). Orbital perturbations of the seasonal cycle are believed to be critical determinants of the long-term behavior of ENSO (*2*). Proxy hydrographic records from the tropical Pacific document significant spectral power at precessional periods [19 to 23 thousand years (ky)] (*3*, *4*), but the specific mechanisms by which precession affects basin-scale ocean-atmosphere dynamics and their interaction with global climate remain elusive. Paleoclimatic evidence bearing on these questions is scant because of a lack of detailed, well-dated climate records from this region. In this study, we focus on the cold tongue of the eastern equatorial Pacific (EEP), where the

[1]Lamont-Doherty Earth Observatory and Department of Earth and Environmental Sciences, Columbia University, Palisades, NY 10964, USA. [2]Department of Earth, Atmospheric, and Planetary Sciences, Massachusetts Institute of Technology, 77 Massachusetts Avenue, Cambridge, MA 02139, USA.

*To whom correspondence should be addressed. E-mail: athan@ldeo.columbia.edu